GABA produced by multiple bone marrow cell types regulates hematopoietic stem and progenitor cells

Cesi Deng (邓策思)[1], Adedamola Elujoba-Bridenstine[1], Ai Tang Song[1], Rylie M. Ceplina[1], Casey J. Ostheimer[1], Molly C. Pellitteri Hahn[2], Cameron O. Scarlett[2], Owen J. Tamplin[1,*]

[1]Department of Cell and Regenerative Biology, School of Medicine and Public Health, University of Wisconsin-Madison, Madison, WI, USA

[2]Analytical Instrumentation Center, School of Pharmacy, University of Wisconsin-Madison, Madison, WI, USA

[*]Corresponding author: tamplin@wisc.edu

Summary

Hematopoietic stem and progenitor cells (HSPCs) maintain homeostasis of the blood system by balancing proliferation and differentiation. Many extrinsic signals in the bone marrow (BM) microenvironment that regulate this balance are still unknown. We report gamma aminobutyric acid (GABA) metabolite produced in the BM as a regulator of HSPCs. Deletion of the glutamate decarboxylase enzymes (Gad1/2) that produce GABA in either B lineages or endothelial cells (ECs) leads to a moderate reduction in BM GABA levels and HSPC number, suggesting both cell types are GABA sources. However, simultaneous blockade of GABA production from both hematopoietic cells and ECs resulted in a greater reduction of both GABA levels and HSPC numbers. Lower GABA levels in the BM altered the gene expression profile of HSPCs, with expression reduced for proliferation-associated genes and increased for B lineage genes. Our findings suggest GABA from multiple sources coordinates to regulate HSPC activity.

25 **Highlights**

26 - GABA is produced by B cells and endothelial cells in the bone marrow
27 - Lower GABA level in the bone marrow reduces HSPC proliferation
28 - Lower GABA level primes HSPCs to upregulate B cell differentiation programs

29

30 **eTOC blurb**

31 Tamplin and colleagues functionally test production of GABA metabolite in the bone marrow
32 microenvironment as a regulator of hematopoietic stem and progenitor cells. Conditional deletion
33 of GAD enzymes in B cells and endothelial cells demonstrated both are sources of GABA. Lower
34 GABA level primed HSPCs to reduce proliferation and upregulate B cell differentiation programs.

35

36 **Introduction**

37 Hematopoietic stem and progenitor cells (HSPCs) replenish the entire blood system throughout
38 life (Pinho and Frenette, 2019). The balance between HSPC proliferation and differentiation is
39 tightly regulated by extrinsic signals in their microenvironment, also known as the niche. In adults,
40 bone marrow (BM) is the primary site of hematopoiesis and is made up of a highly complex array
41 of different niche cell types. Although research has focused on the cytokines, other growth factors,
42 receptor ligands, and adhesion molecules produced by these different niche cells, there are also
43 understudied factors such as metabolites and neurotransmitters that play a role in regulating HSPC
44 activity. For example, peripheral nerves can provide adrenergic signals that act on stromal cells to
45 regulate HSPC mobilization (Méndez-Ferrer et al., 2008), and dopamine can act directly acting on
46 neuroreceptors on the HSPC surface (Liu et al., 2021). The full range of secreted immune
47 metabolites are reviewed elsewhere (Zhang et al., 2022).

48 Gamma amino-butyric acid (GABA) is a major neurotransmitter in the central nervous system.
49 GABA binds to two classes of receptors, ionotropic $GABA_A$ receptor and metabotropic $GABA_B$
50 receptor. Interestingly, both types of GABA receptors have been found on HSPCs. GABA type A
51 receptor subunit rho 1 (GABRR1) marks a subset of HSPCs and its deletion inhibited
52 megakaryocyte differentiation and reduced blood platelets (Zhu et al., 2019). In our previous work,
53 we showed that loss of GABA type B receptor subunit 1 (GABBR1) reduced proliferation and
54 reconstitution capacity of hematopoietic stem cells (HSCs), and impaired B cell production (Shao
55 et al., 2021). While these findings suggest GABA has a pleiotropic role in regulating HSPC activity,
56 the sources of GABA in the BM remain unclear. We examined the spatial distribution of GABA in
57 the BM using imaging mass spectrometry and found it was enriched in the endosteal region of the
58 mouse femur (Shao *et al.*, 2021). GABA production is catalyzed by glutamate decarboxylases 1

59 and 2 (GAD1/2) (Erlander et al., 1991). Work by us and others showed *GAD1* but not *GAD2* is
60 expressed in human and mouse B cells that are also enriched for GABA metabolite (Shao et al.,
61 2021, Zhang et al. 2021). We sought to block GABA production from various bone marrow niche
62 cell types. We show that B cells and endothelial cells produce GABA, which is required for the
63 maintenance of the HSPC pool. HSPCs are primed to commit to the B cell lineage when GABA
64 level in the microenvironment is low. We propose that GABA serves as an environmental cue to
65 regulate the decision between HSPC proliferation and B cell production to maintain homeostasis
66 of the B cell pool.

67

68 **Results**

69 *B cells are a source of GABA in the bone marrow niche*

70 To determine if B cells are an autonomous source of GABA, we tracked GABA production
71 throughout B cell development using the OP9 stromal cell co-culture system (Holmes and Zuniga-
72 Pflucker, 2009; Shao *et al.*, 2021). In brief, HSPCs (Lin-/c-Kit+/Sca-1+) sorted from wild-type
73 (WT) mice were co-cultured with stromal cells and examined at 3-day intervals. GABA level in
74 the co-culture media was determined by mass spectrometric analysis, and B lineage cell production
75 was determined by flow cytometry (Fig. 1A-B). We found Cd19+ cells emerged on Day 9 and
76 underwent rapid expansion in the following three days (Fig. 1A-C). Our baseline was GABA level
77 in media and OP9 cells alone that do not produce GABA, to normalize against the small amount
78 of GABA present in fetal bovine serum. During B cell differentiation the GABA level remained
79 low until Day 9 and then increased dramatically at Day 12 (Fig. 1C). The synchronization of B
80 lineage cell emergence and GABA production demonstrated B cells are a source of GABA. This

81 autonomous production of GABA by B cells during differentiation was consistent with the results
82 of others that detected GABA in B cells purified from human peripheral blood and mouse lymph
83 nodes (Zhang et al., 2021).

84 To confirm the *in vivo* functional requirement of GABA production by B cells in the bone marrow
85 niche, we generated mouse models with B cell-specific deletion of *Gad1/2*. We crossed *Cd19-Cre*
86 (Rickert et al., 1997) and *Gad1/2*$^{fl/fl}$*;Rosa26*^{tdTomato} mouse lines (Meng et al., 2016) to generate
87 *Cd19-cre;Gad1/2*$^{fl/fl}$*;Rosa26*^{tdTomato} (Fig. 1D). *Cd19-Cre* activity was shown by the percentage of
88 double positive Cd19+/tdTomato+ cells (Fig. S1A). We isolated HSPCs from *Cd19-*
89 *cre;Gad1/2*$^{fl/fl}$*;Rosa26*^{tdTomato} mice and induced their differentiation into B cells using the OP9 co-
90 culture system. There was significant reduction of GABA level in co-cultures seeded with HSPCs
91 from *Cd19-cre;Gad1/2*$^{fl/fl}$*;Rosa26*^{tdTomato} mice (Fig. 1E).

92 We used mass spectrometry to measure GABA levels in femurs from *Cd19-*
93 *Cre;Gad1/2*$^{fl/fl}$*;Rosa26*^{tdTomato} mice but did not find a significant difference compared to controls
94 (Fig. 1F). Consistent with previously published results that used the B lineage-specific conditional
95 *Gad1* knockout model *Mb1-Cre;Gad1*$^{fl/fl}$ (Zhang *et al.*, 2021), we also observed no change in BM
96 HSPC numbers, number of BM B220+ cells, or percentage of BM and peripheral blood (PB)
97 B220+ cells (Fig. S2A-C). Interestingly, we did observe a decrease in the proportion of BM HSPCs
98 (Fig. 1G), a phenotype that was not tested in the *Mb1-Cre;Gad1*$^{fl/fl}$ model (Zhang *et al.*, 2021),
99 suggesting B cell-derived GABA may directly regulate HSPCs.

100 <u>Endothelial cells are a source of GABA in the bone marrow niche</u>

101 Data from our group and others found bone marrow endothelial cells (BMECs) express *Gad1* and
102 are therefore a potential source of GABA (Shao *et al.*, 2021; Zhu *et al.*, 2019). Notably, published

103 mouse bone marrow stroma single cell RNA-seq datasets do not show *Gad1* expression in any
104 populations (Baryawno et al., 2019), while quantitative PCR and bulk RNA-seq detect its
105 expression in B cells and BMECs (Shao *et al.*, 2021; Zhang *et al.*, 2021; Zhu *et al.*, 2019),
106 suggesting *Gad1* transcript may be expressed at low levels. To functionally test if ECs contribute
107 to GABA production in BM, we generated an endothelial-specific *Gad1/2* deletion by crossing
108 *Cdh5-CreERT2* (Sörensen et al., 2009) and *Gad1/2*$^{fl/fl}$*;Rosa26*^{tdTomato} lines to generate *Cdh5-*
109 *CreERT2;Gad1/2*$^{fl/fl}$*;Rosa26*^{tdTomato} mice (Fig. 2A). Tamoxifen was administered at 5-6 weeks and
110 experiments were performed at 8-12 weeks. *Cdh5-CreERT2* activity was confirmed by the
111 presence of tdTomato+ cells in the BM (Fig. S1B). There was no significant decrease in GABA
112 levels in *CreERT2;Gad1/2*$^{fl/fl}$*;Rosa26*^{tdTomato} BM (Fig. 2B); however, there was a reduction in both
113 number and proportion of HSPCs (Fig. 2C). No change was detected in BM cellularity, CLPs or
114 B cells, or PB myeloid or B cells (Fig. S2D-H). These results demonstrated that *Gad1/2* deletion
115 from BMECs did not broadly impact BM hematopoiesis or GABA levels, however it was sufficient
116 to modulate the proportion and number of HSPCs.

117 <u>Hematopoietic and BMEC-derived GABA coordinates to regulate HSPC activity</u>

118 To understand the contribution of multiple sources of GABA in the BM, we generated a *Tie2-*
119 *Cre;Gad1/2*$^{fl/fl}$*;Rosa26*^{tdTomato} mouse model (Fig. 3A). *Tie2-Cre* is expressed in all ECs during
120 embryonic development and into adulthood (Kisanuki et al., 2001). In the embryo, the hemogenic
121 endothelium gives rise to all definitive HSPCs, meaning in the adult *Tie2-cre* model all ECs and
122 hematopoietic cells have undergone Cre excision (Tang et al., 2010). Therefore, the *Tie2-*
123 *Cre;Gad1/2*$^{fl/fl}$*;Rosa26*^{tdTomato} mouse model enabled us to evaluate the effect of *Gad1/2* deletion in
124 all ECs and hematopoietic cells, inclusive of both B cells and BMECs. Cre activity was confirmed
125 by detection of tdTomato+ cells in the BM (Fig. S1C). We measured GABA levels in the BM of

126 *Tie2-Cre;Gad1/2*$^{fl/fl}$*;Rosa26*^{tdTomato} mice and detected a ~60% reduction compared to control mice
127 (Fig. 3B). Considering that deletion of *Gad1/2* from B cells (Fig. 1F) or ECs alone (Fig. 2B) did
128 not lead to a significant reduction of BM GABA, our results using the *Tie2-Cre* model suggest B
129 cells and BMECs synergize to sustain homeostatic BM GABA levels. As in the EC-specific *Cdh5-*
130 *CreERT2;Gad1/2*$^{fl/fl}$*;Rosa26*^{tdTomato} model (Fig. 2C), we found a decrease in HSPC percentage and
131 number in *Tie2-Cre;Gad1/2*$^{fl/fl}$*;Rosa26*^{tdTomato} BM (Fig. 3C). We did not observe any changes in
132 BM cellularity, CLPs, or B220+ cells, or PB myeloid cells (Fig. S2I-L). We did observe a slight
133 reduction in the percentage of PB B220+ cells (Fig. 3D). Although the *Cd19-Cre*, *Cdh5-CreERT2*,
134 and *Tie2-Cre* models all showed a decrease in the proportion of BM HSPCs, only the combined
135 hematopoietic and EC-specific deletion of *Gad1/2* with *Tie2-Cre* resulted in a significant reduction
136 in BM GABA levels. This shows that GABA is produced by multiple sources at steady state to
137 regulate HSPC activity in the BM niche.

138 <u>Reduced BM GABA levels induced a shift in gene expression profiles of HSPCs</u>

139 To determine if attenuated BM GABA levels result in intrinsic molecular changes in HSPCs, we
140 isolated HSPCs from *Cd19-Cre*, *Cdh5-CreERT2*, and *Tie2-Cre;Gad1/2*$^{fl/fl}$*;Rosa26*^{tdTomato} models
141 and performed bulk RNA-sequencing. Among the total 21,114 genes detected, there were
142 differentially expressed genes (DEGs) in HSPCs of each model when compared to WT: 494 in
143 *Cd19-Cre* (367 upregulated, 127 downregulated); 284 in *Cdh5-CreERT2* (131 upregulated, 153
144 downregulated); 200 in *Tie2-Cre* (73 upregulated, 127 downregulated; FDR < 0.1, |log2FC| > 1;
145 Fig. 4A-B, Fig. S3A). Comparison of DEGs in each mutant showed 21 genes were commonly
146 upregulated upon GABA level reduction, including HSC genes *Hlf*, *Emcn*, and *Fgd5* (Fig. 4A-C)
147 (Calvanese et al., 2022; Engelhard et al., 2024; Gazit et al., 2014; Holmfeldt et al., 2016; Matsubara

148 et al., 2005; Reckzeh et al., 2018; Ueno et al., 2001). Together, this demonstrates that HSPCs
149 respond to changes in GABA produced by BMECs and hematopoietic cells.

150 Our previous analysis of GABA receptor *Gabbr1* loss-of-function mutant HSPCs found they were
151 less proliferative, less responsive to poly(I:C), and had defective B cell differentiation (Shao *et al.*,
152 2021). Intriguingly, phenotypic *Gabbr1* null HSPCs exhibited a shift in transcriptional profiles
153 from undifferentiated progenitor to more B lineage committed progenitor (Shao *et al.*, 2021). We
154 hypothesized loss of *Gabbr1* in HSPCs would simulate attenuated GABA signaling and therefore
155 may mimic HSPCs from a low GABA microenvironment. To test this, we considered DEGs
156 separately in the *Cd19-Cre*, *Cdh5-CreERT2*, and *Tie2-Cre* models and performed gene set
157 enrichment analysis (GSEA) for HSPCs from each model (Fig. 4D,E; Fig. S3C-E; Supplementary
158 Tables). Like *Gabbr1* null HSPCs, we found B cell receptor signaling pathway and B cell
159 activation were enriched in all compared to WT (Fig. S3C-E). We also found interferon signaling
160 pathways were highly upregulated in all *Gad1/2*$^{fl/fl}$ models (Fig 4D). This is consistent with our
161 previous finding that showed a positive correlation between *Gabbr1* expression in HSPCs and the
162 expression of genes related to interferon signaling (Shao *et al.*, 2021), further supporting the
163 GABA-GABBR1 axis in regulating HSPC differentiation and immune response. Consistent with
164 reduced proliferative capacity, E2F and MYC targets, and G2M checkpoint genes were under-
165 represented in *Gad1/2*$^{fl/fl}$ models compared to WT (Fig 4E). Together, this showed that phenotypic
166 HSPCs from a low GABA microenvironment have a similar intrinsic profile to HSPCs that lack
167 GABBR1 receptor signaling.

168 There were many similarities between *CD19-Cre*, *Cdh5-CreERT2*, and *Tie2-Cre* models, however
169 we wanted to consider if there were differences in HSPC regulation that were dependent on the
170 cellular source of GABA. The hierarchical clustering of DEGs from all models showed clusters

171 that were unique to B lineages, BMECs, or both (Fig. 4A). Intriguingly, a curated list of B lineage
172 genes (Miyai et al., 2018) found some of these markers were only strongly upregulated in the
173 *Cd19-Cre* model (e.g., *Cd79a, Cd79b, Vpreb1*; Fig. S3B; Supplementary Tables). *Mecom*, an
174 important regulator of HSCs (Voit et al., 2023), was only upregulated in models that deleted
175 *Gad1/2* from BMECs (i.e., *Cdh5-CreERT2 and Tie2-Cre*). These findings suggest that HSPCs may
176 be differentially regulated by GABA depending on their location in the BM niche, and their
177 proximity to B cells or BMECs. Together, our data shows reduced production of GABA in the BM
178 niche promotes HSPC priming towards B cell lineage commitment, while suppressing HSPC
179 proliferation. Overall, our results reveal a role for GABA as a molecular switch to regulate HSPC
180 activity and B lineage priming.

181 Based on our previous finding that GABBR1 is required for HSPC proliferation and B cell
182 differentiation (Shao *et al.*, 2021), we hypothesized there may be a feedback loop between
183 Gad1/2+ B cells and GABBR1+ HSPCs, with lower GABA levels favoring HSPC to B cell lineage
184 differentiation, and higher GABA levels driving HSPC proliferation. Previously, we showed that
185 human CD34+ umbilical cord blood (UCB) HSPCs could be stimulated *ex vivo* with a short two
186 hour treatment using the GABBR1 agonist Baclofen, which improved long-term
187 xenotransplantation in immunodeficient mice (Shao *et al.*, 2021). Therefore, we considered
188 sustained suppression of GABBR1 signaling with the antagonist 2-OH-Saclofen could favor B cell
189 production. We tested multiple doses of 2-OH-Saclofen in B cell differentiation OP9 co-cultures
190 and found a range of doses from 0.5-5.0 μM increased B cell production 3-fold (Fig. 4F). These
191 results show the GABA-GABBR1 axis is tunable to balance HSPC proliferation and B lineage
192 differentiation.

193

194 **Discussion**

195 GABA is well-known as an inhibitory neurotransmitter in the central nervous system, but it has
196 also been detected in peripheral organs, including peripheral nervous system, gastrointestinal track,
197 pancreas and liver (Zhang *et al.*, 2022). In these peripheral tissues, GABA has diverse functions
198 beyond transmitting neural signals, such as regulating immune cell activity in lymph nodes. We
199 showed that GABA serves as an environmental cue in the bone marrow to regulate HSPC
200 differentiation into B cells and maintain the stem cell pool. Despite detectable GABA in multiple
201 peripheral tissues, the sources of GABA remain largely unknown. We show here that B cells and
202 BMECs synergize to maintain homeostatic levels of GABA. Interestingly, GABA level in the BM
203 was not fully reduced even when *Gad1/2* was deleted from both hematopoietic cells and ECs using
204 the *Tie2-Cre* model, suggesting other unknown GABA sources. A survey of published mouse BM
205 stromal cell single cell RNA-seq datasets did not identify any cells that express *Gad1* or *Gad2*
206 (Baryawno *et al.*, 2019), possibly because mRNA expression levels are below the limit of detection
207 using this method. While GAD1 is considered the primary pathway for GABA biosynthesis, other
208 mechanisms have been found, including catalysis of putrescine by aldehyde dehydrogenases (Kim
209 et al., 2015; Li et al., 2025). Further investigation will be needed to identify all the sources of
210 GABA production in the BM microenvironment.

211 HSPCs sorted from the BM of *CD19-Cre*, *Cdh5-CreERT2*, and *Tie2-Cre* models shared many
212 phenotypic similarities. This included an upregulation of immune response genes, including
213 immunoglobulin genes and B cell blueprint genes. This observation was consistent with
214 phenotypic HSPCs sorted from *Gabbr1* null mutant BM, where later-stage B cell commitment
215 genes and pro-B cell-signature genes were highly upregulated (Shao *et al.*, 2021). Strikingly,
216 HSPCs from our *Gad1/2*-deficient BM niche models also had downregulation of genes associated

217 with proliferation, another hallmark of *Gabbr1* null mutant HSPCs. These shared changes in
218 HSPCs that lack the GABBR1 receptor, or reside in BM with lower GABA levels, suggests the
219 GABA-GABBR1 axis is important for balancing a decision between HSPC proliferation and
220 differentiation, specifically towards B lineages.

221 Although we observed many similarities in HSPCs from different *Gad1/2*-deficient BM niche
222 models, there were differences as well, such as B lineage-specific genes *Cd79a*, *Cd79b*, and
223 *Vpreb1* that were uniquely upregulated in *Cd19-cre*$^{+}$*;Gad1/2*$^{fl/fl}$ mutant HSPCs. These
224 transcriptional differences likely arise from the blockade of GABA production in different niche
225 cell types. Spatial mapping of lymphopoiesis in the sternum has revealed that common lymphoid
226 progenitors (CLPs) reside in an arteriolar niche, surrounded by Pre-Pro-B, Pro-B and Pre-B cells
227 (Wu et al., 2024). Within this B cell production line, more lineage-committed cells are located
228 further away from CLPs, suggesting spatial heterogeneity in GABA production. While both
229 endothelial cells and B lineage cells are GABA sources, lymphoid progenitors are proximal to
230 arterioles and more distant from Pro-B and Pre-B cells (Wu *et al.*, 2024). Therefore, the blockade
231 of GABA production from either or both sources could differentially impact HSPC activity
232 depending on their spatial relationships. Understanding the spatial heterogeneity of niche factors
233 will provide more insights into how specialized niches support hematopoiesis.

234 Downstream differentiated hematopoietic cells have been recognized as regulators of their own
235 upstream HSPCs through feedback mechanisms (Kirouac et al., 2010). For example, platelet-
236 biased vWF + HSCs associate with megakaryocyte niches and are regulated by CXCL4 produced
237 by megakaryocytes (Pinho et al., 2018). We demonstrate here that GABA-producing B cells
238 regulate GABBR1+ HSPCs, emphasizing the importance of feedback mechanisms in the bone
239 marrow niche to maintain homeostasis. Pharmacological modulation of these mechanisms could

240 lead to repurposing of clinical neuromodulators to target the hematopoietic and immune systems

241 for therapeutic benefits.

242

243 **Methods**

244 *Mice*

245 Cd19-Cre (JAX stock #006785) (Rickert *et al.*, 1997), *Tie2-Cre* (JAX stock #004128) (Koni et al.,
246 2001), *Gad1*^{lox}*::Gad2*^{lox}*::Rosa26*^{tdTomato} (JAX stock #031800) (Meng *et al.*, 2016), and C57BL/6
247 mice were purchased from the Jackson Laboratory. *Cdh5-CreERT2* was generated by Ralf Adam's
248 group (Sörensen *et al.*, 2009). To generate *Gad1/2* deletion in different cell types, *Cd19-Cre*, *Cdh5-*
249 *CreERT2*, and *Tie2-Cre* were bred to *Gad1*^{lox}*::Gad2*^{lox}*::Rosa26*^{tdTomato}. Genotyping was performed
250 by Transnetyx. At 5-6 weeks of age, *Cdh5-CreERT2;Gad1/2*$^{fl/fl}$ mice or Cre-negative littermate
251 controls were injected with 1.5 mg Tamoxifen (Sigma, T5648; dissolved in medium chain fatty
252 acids (Sigma, C8267)) at 10 mg/mL per day for 5 consecutive days to induce Cre activity. Both
253 male and female mice between 8-12 weeks of age were used in all the studies. All mice were
254 housed in the breeding core at the University of Wisconsin-Madison. All protocols were approved
255 by the University of Wisconsin-Madison Institutional Animal Care and Use Committee.

256 *Flow cytometry of hematopoietic populations*

257 Femurs and tibias were harvested from 8-12 week-old mice and crushed in phosphate-buffered
258 saline (PBS, Corning, 21-040-CV) containing 2% heat inactivated fetal bovine serum with mortar
259 and pestle. PB was collected by cardiac puncture. RBCs were removed by lysis with BD
260 PharmLyse Lysing Buffer (BD Biosciences, 555899). For HSPC isolation, BM cells were pre-
261 enriched for c-Kit+ cells using c-Kit microBeads (Miltenyi Biotec, 130-091-224) and a Midi
262 MACS separator (Miltenyi Biotec, 130-042-301). BM, PB, or c-Kit-enriched cells were then
263 stained for 30 min at 4°C with combinations of antibodies to the following cell surface markers
264 conjugated with different fluorochromes: CD3 (BioLegend, 17A2), CD11b (BioLegend, M1/70),

265 Ter119 (BioLegend, TER119), Gr1 (BioLegend, RB6-8C5), B220 (BioLegend, RA3-6B2), c-Kit
266 (BioLegend, 2B8), Sca-1 (BioLegend, D7), CD127 (BioLegend, SB/199), CD135 (BioLegend,
267 A2F10). HSPC isolation was performed on BD FACSAria and BD FACSDiscover S8 Cell sorters.
268 Data collection was performed on BD LSRII Fortessa and data analysis was performed using
269 FlowJo v10.10.

270 *Mass spectrometric detection of GABA*

271 For LC/MS/MS analysis of GABA, mouse bones were prepared by homogenization, precipitation,
272 and filtration. Details are provided in Supplementary Methods.

273 *In vitro B cell differentiation assay*

274 OP9 stromal cells were purchased from American Type Culture Collection (CRL-2749) and were
275 grown as previously described (Shao *et al.*, 2021). 4,000 HSPCs from WT or *Gad1/2* KO mice
276 were sorted onto a monolayer of cells with 1 ml DMEM medium containing 10% FBS, 5 ng/ml
277 Flt-3L (PeproTech, 250-31L) and 1 ng/ml IL-7 (R&D Systems, 407-ML-005). GABA (R&D
278 Systems, 0344) or GABBR1 antagonist 2-OH-Saclofen (Tocris Biosciences, 0245) were added at
279 appropriate concentrations to the media. After 7 days of co-culturing, hematopoietic cells were
280 mechanically detached, filtered and transferred to fresh OP9 monolayers. Cells were harvested 12
281 days after initial culturing and stained with Cd45 (BioLegend, 30-F11), B220 (BioLegend, RA3-
282 6B2), Cd19 (BioLegend, 6D5) and Cd11b (Biolegend, M1/70) antibodies. Cells were analyzed by
283 brightfield microscopy Nikon ECLIPSE TS2 and flow cytometry. Conditioned media was
284 analyzed by mass spectrometry. Cell counts were determined by hemacytometer. For time course
285 experiments, cells were harvested and analyzed at 3-day intervals after initiation of co-cultures.
286 Flow cytometry analysis was performed using BD LSRII Fortessa and FlowJo v9/10.10.

287 *Bulk RNA-seq library preparation and sequencing*

288 LSK cells from 8-12 week-old wild-type or *Cd19-Cre;Gad1/2*$^{fl/fl}$, *Cdh5-CreERT2;Gad1/2*$^{fl/fl}$, and
289 *Tie2-Cre;Gad1/2*$^{fl/fl}$ models (triplicates for each group) were sorted using BD FACSAria Cell
290 Sorter or BD FACSDiscover S8 Cell Sorter and collected in Trizol LS (Invitrogen). Nuclease-free
291 water was added to adjust the volume to a final ratio of 3:1 for Trizol LS and sample. Samples
292 were stored at -80°C until ready for RNA extraction. Samples were thawed, equilibrated to room
293 temperature, and 100 uL nuclease-free water was added to each sample to reduce the density of
294 aqueous phase. 5PRIME Phase Lock Gel tubes (Quantabio) were used following the manufacturer
295 instructions to separate the aqueous phase. Once the aqueous phase was separated, 25 ug of
296 GenElute-LPA (Sigma, Cat.56575) was added to each sample for RNA precipitation. After adding
297 isopropanol, samples were stored overnight at -20°C for RNA precipitation. The pellet was then
298 washed three times with 75% ethanol, resuspended in 10 uL nuclease-free water, and stored at -
299 80°C until library preparation.

300 RNA samples were quantified, and integrity was examined using Agilent 2100 Bioanalyzer RNA
301 PicoChip. RNA libraries were prepared by UW-Madison Gene Expression Center using Takara
302 SMARTer Stranded RNA v2 Prep Kit - Pico Input Mammalian (Takara Bio). RNA input for library
303 preparation was 1-2.5 ng. The quality of libraries was examined using Agilent 4200 TapeStation.
304 Sequencing was run on an Illumina NovaSeq X Plus single 2x150 bp lane at the UW-Madison
305 Next Generation Sequencing Core.

306 *Bulk RNA-Seq analysis*

307 Raw reads were checked for quality (FastQC v0.12.1) and adapter sequences were trimmed. Reads
308 were mapped to the mouse reference genome GRCm39 using STAR aligner and read counts were

309 normalized using RSEM by the UW-Madison Bioinformatics Resource Core. Low expression
310 genes were filtered, library size was normalized and DGE (Differential Gene Expression) analysis
311 was performed using EdgeR (v4.4.2). Principal component analysis identified an outlier that was
312 removed from further analysis. The final analysis included n=3 samples of sorted HSPCs from WT,
313 *Tie2-Cre;Gad1/2*$^{fl/fl}$, and *Cdh5-CreERT2;Gad1/2*$^{fl/fl}$ BM samples, and n=2 from *Cd19-*
314 *Cre;Gad1/2*$^{fl/fl}$. Pairwise comparisons between WT samples and each mutant were performed using
315 the quasi-likelihood F-test and genes with Log2 Fold Change > 1 and False Discovery Rate (FDR)
316 < 0.1 were selected as DE genes. For heatmaps depicting unsupervised hierarchical clustering,
317 genes that were differentially expressed in at least one mutant were used with the following
318 parameters. GSEA (Gene Set Enrichment Analysis) of HSPCs isolated from mutants was
319 performed using clusterProfiler (release 3.21) with GseaPreranked method. MSigDB Gene sets
320 were downloaded using R package msigdbr (v7.5.1). Gene sets used for GSEA included
321 HALLMARK and GO:BP sets. Rank scores for each pairwise comparison were created by
322 multiplying the negative log of the p-value by the sign of the log fold change and ranking in
323 descending order. A cutoff of adjusted p value < 0.05 was applied for GSEA and results were
324 further filtered using the following criteria: adjusted p-value < 0.01, setSize >= 15 and <= 301,
325 abs(NES) >= 2. Data was submitted to NCBI GEO under the accession number GSE294951.

326 *Statistics*

327 The data was presented as mean ± sd. For the comparison between single experimental and control
328 groups, Welch's t test was used. For comparison between multiple groups, Analysis of Variance
329 (ANOVA) was used, and Tukey's HSD was used as the post-hoc test to determine differences
330 between groups. P < 0.05 is considered as statistical significance. GraphPad Prism 10.4 was used
331 for all analyses.

332 **Acknowledgments**

333 The authors thank the University of Wisconsin Carbone Cancer Center Flow Cytometry
334 Laboratory, supported by P30 CA014520, for use of its facilities and services, especially Kathryn
335 Fox and Zach Stenerson for their technical assistance with panel optimization; Kathy Krentz at
336 University of Wisconsin-Madison Animal Models Core for mouse model rederivation and
337 cryopreservation; Megan Latsch and Jody Peter of the University of Wisconsin Biomedical
338 Research Model Services for mouse colony management; Lauren Wells and Sandra Splinter
339 BonDurant at University of Wisconsin-Madison Biotechnology Gene Expression Center
340 (Research Resource Identifier – RRID:SCR_017757) for bulk RNA-sequencing library
341 preparation; University of Wisconsin-Madison Next Gen DNA Sequencing Core for Illumina
342 sequencing; Mark E. Berres at University of Wisconsin-Madison Biotechnology Center
343 Bioinformatics Core Facility (Research Resource Identifier – RRID:SCR_017799) for sequencing
344 reads alignment. Flow cytometry analyses and cell sorting utilized instruments that were supported
345 by the following grants: BD LSR Fortessa (1S10OD018202-01), BD FACS AriaII BSL-2 Cell
346 Sorter, "Jill" (1S10RR025483-01). Research reported in this publication was supported by the
347 American Society of Hematology (ASH Bridge Grant) and the Department of Cell and
348 Regenerative Biology at the University of Wisconsin-Madison.

349

350 **Author contributions**

351 Conceptualization, O.J.T.; Data curation, C.D.; Formal Analysis, C.D., A.E.-B., M.P.H.; Funding
352 Acquisition, O.J.T.; Investigation, C.D., A.E.-B., A.T.S., R.M.C., C.J.O., M.P.H., C.O.S.;
353 Methodology, M.P.H., C.O.S.; Project Administration, O.J.T.; Resources, O.J.T.; Software, C.D.;

Supervision, O.J.T.; Validation, C.D.; Visualization, C.D. and A.E.-B.; Writing - Original draft, C.D.; Writing – reviewing and editing, O.J.T..

Declaration of interests

The authors declare no competing interests.

References

Baryawno, N., Przybylski, D., Kowalczyk, M.S., Kfoury, Y., Severe, N., Gustafsson, K., Kokkaliaris, K.D., Mercier, F., Tabaka, M., Hofree, M., et al. (2019). A Cellular Taxonomy of the Bone Marrow Stroma in Homeostasis and Leukemia. Cell *177*, 1915-1932 e1916. 10.1016/j.cell.2019.04.040.

Calvanese, V., Capellera-Garcia, S., Ma, F., Fares, I., Liebscher, S., Ng, E.S., Ekstrand, S., Aguade-Gorgorio, J., Vavilina, A., Lefaudeux, D., et al. (2022). Mapping human haematopoietic stem cells from haemogenic endothelium to birth. Nature *604*, 534-540. 10.1038/s41586-022-04571-x.

Engelhard, S., Estruch, M., Qin, S., Engelhard, C.A., Rodriguez-Gonzalez, F.G., Drilsvik, M., Martin-Gonzalez, J., Lu, J.W., Bryder, D., Nerlov, C., et al. (2024). Endomucin marks quiescent long-term multi-lineage repopulating hematopoietic stem cells and is essential for their transendothelial migration. Cell Rep *43*, 114475. 10.1016/j.celrep.2024.114475.

Erlander, M.G., Tillakaratne, N.J., Feldblum, S., Patel, N., and Tobin, A.J. (1991). Two genes encode distinct glutamate decarboxylases. Neuron *7*, 91-100.

Gazit, R., Mandal, P.K., Ebina, W., Ben-Zvi, A., Nombela-Arrieta, C., Silberstein, L.E., and Rossi, D.J. (2014). Fgd5 identifies hematopoietic stem cells in the murine bone marrow. The Journal of experimental medicine *211*, 1315-1331. 10.1084/jem.20130428.

Holmes, R., and Zuniga-Pflucker, J.C. (2009). The OP9-DL1 system: generation of T-lymphocytes from embryonic or hematopoietic stem cells in vitro. Cold Spring Harbor protocols *2009*, pdb.prot5156. 10.1101/pdb.prot5156.

Holmfeldt, P., Ganuza, M., Marathe, H., He, B., Hall, T., Kang, G., Moen, J., Pardieck, J., Saulsberry, A.C., Cico, A., et al. (2016). Functional screen identifies regulators of murine hematopoietic stem cell repopulation. J Exp Med *213*, 433-449. 10.1084/jem.20150806.

Kim, J.I., Ganesan, S., Luo, S.X., Wu, Y.W., Park, E., Huang, E.J., Chen, L., and Ding, J.B. (2015). Aldehyde dehydrogenase 1a1 mediates a GABA synthesis pathway in midbrain dopaminergic neurons. Science *350*, 102-106. 10.1126/science.aac4690.

Kirouac, D.C., Ito, C., Csaszar, E., Roch, A., Yu, M., Sykes, E.A., Bader, G.D., and Zandstra, P.W. (2010). Dynamic interaction networks in a hierarchically organized tissue. Molecular systems biology *6*, 417. 10.1038/msb.2010.71.

Kisanuki, Y.Y., Hammer, R.E., Miyazaki, J., Williams, S.C., Richardson, J.A., and Yanagisawa, M. (2001). Tie2-Cre transgenic mice: a new model for endothelial cell-lineage analysis in vivo. Dev Biol *230*, 230-242. 10.1006/dbio.2000.0106.

Koni, P.A., Joshi, S.K., Temann, U.A., Olson, D., Burkly, L., and Flavell, R.A. (2001). Conditional vascular cell adhesion molecule 1 deletion in mice: impaired lymphocyte migration to bone marrow. J Exp Med *193*, 741-754. 10.1084/jem.193.6.741.

Li, L., Kang, Y., Cheng, R., Liu, F., Wu, F., Liu, Z., Kou, J., Zhang, Z., Li, W., Zhao, H., et al. (2025). The de novo synthesis of GABA and its gene regulatory function control hepatocellular carcinoma metastasis. Dev Cell *60*, 1053-1069 e1056. 10.1016/j.devcel.2024.12.007.

Liu, Y., Chen, Q., Jeong, H.W., Han, D., Fabian, J., Drexler, H.C.A., Stehling, M., Scholer, H.R., and Adams, R.H. (2021). Dopamine signaling regulates hematopoietic stem and progenitor cell function. Blood *138*, 2051-2065. 10.1182/blood.2020010419.

Matsubara, A., Iwama, A., Yamazaki, S., Furuta, C., Hirasawa, R., Morita, Y., Osawa, M., Motohashi, T., Eto, K., Ema, H., et al. (2005). Endomucin, a CD34-like sialomucin, marks hematopoietic stem cells throughout development. J Exp Med *202*, 1483-1492. 10.1084/jem.20051325.

Méndez-Ferrer, S., Lucas, D., Battista, M., and Frenette, P.S. (2008). Haematopoietic stem cell release is regulated by circadian oscillations. Nature *452*, 442-447. 10.1038/nature06685.

Meng, F., Han, Y., Srisai, D., Belakhov, V., Farias, M., Xu, Y., Palmiter, R.D., Baasov, T., and Wu, Q. (2016). New inducible genetic method reveals critical roles of GABA in the control of feeding and metabolism. Proc Natl Acad Sci U S A *113*, 3645-3650. 10.1073/pnas.1602049113.

Miyai, T., Takano, J., Endo, T.A., Kawakami, E., Agata, Y., Motomura, Y., Kubo, M., Kashima, Y., Suzuki, Y., Kawamoto, H., and Ikawa, T. (2018). Three-step transcriptional priming that drives the commitment of multipotent progenitors toward B cells. Genes & development *32*, 112-126. 10.1101/gad.309575.117.

Pinho, S., and Frenette, P.S. (2019). Haematopoietic stem cell activity and interactions with the niche. Nat Rev Mol Cell Biol *20*, 303-320. 10.1038/s41580-019-0103-9.

Pinho, S., Marchand, T., Yang, E., Wei, Q., Nerlov, C., and Frenette, P.S. (2018). Lineage-Biased Hematopoietic Stem Cells Are Regulated by Distinct Niches. Dev Cell *44*, 634-641 e634. 10.1016/j.devcel.2018.01.016.

Reckzeh, K., Kizilkaya, H., Helbo, A.S., Alrich, M.E., Deslauriers, A.G., Grover, A., Rapin, N., Asmar, F., Gronbaek, K., Porse, B., et al. (2018). Human adult HSCs can be discriminated from lineage-committed HPCs by the expression of endomucin. Blood Adv *2*, 1628-1632. 10.1182/bloodadvances.2018015743.

Rickert, R.C., Roes, J., and Rajewsky, K. (1997). B lymphocyte-specific, Cre-mediated mutagenesis in mice. Nucleic Acids Res *25*, 1317-1318. 10.1093/nar/25.6.1317.

Shao, L., Elujoba-Bridenstine, A., Zink, K.E., Sanchez, L.M., Cox, B.J., Pollok, K.E., Sinn, A.L., Bailey, B.J., Sims, E.C., Cooper, S.H., et al. (2021). The neurotransmitter receptor Gabbr1 regulates proliferation and function of hematopoietic stem and progenitor cells. Blood *137*, 775-787. 10.1182/blood.2019004415.

Sörensen, I., Adams, R.H., and Gossler, A. (2009). DLL1-mediated Notch activation regulates endothelial identity in mouse fetal arteries. Blood *113*, 5680-5688. 10.1182/blood-2008-08-174508.

Tang, Y., Harrington, A., Yang, X., Friesel, R.E., and Liaw, L. (2010). The contribution of the Tie2+ lineage to primitive and definitive hematopoietic cells. Genesis *48*, 563-567. 10.1002/dvg.20654.

Ueno, M., Igarashi, K., Kimura, N., Okita, K., Takizawa, M., Nobuhisa, I., Kojima, T., Kitamura, T., Samulowitz, U., Vestweber, D., et al. (2001). Endomucin is expressed in embryonic dorsal aorta and is able to inhibit cell adhesion. Biochem Biophys Res Commun *287*, 501-506. 10.1006/bbrc.2001.5587.

Voit, R.A., Tao, L., Yu, F., Cato, L.D., Cohen, B., Fleming, T.J., Antoszewski, M., Liao, X., Fiorini, C., Nandakumar, S.K., et al. (2023). A genetic disorder reveals a hematopoietic stem cell regulatory network co-opted in leukemia. Nat Immunol *24*, 69-83. 10.1038/s41590-022-01370-4.

Wu, Q., Zhang, J., Kumar, S., Shen, S., Kincaid, M., Johnson, C.B., Zhang, Y.S., Turcotte, R., Alt, C., Ito, K., et al. (2024). Resilient anatomy and local plasticity of naive and stress haematopoiesis. Nature *627*, 839-846. 10.1038/s41586-024-07186-6.

Zhang, B., Vogelzang, A., and Fagarasan, S. (2022). Secreted immune metabolites that mediate immune cell communication and function. Trends Immunol *43*, 990-1005. 10.1016/j.it.2022.10.006.

Zhang, B., Vogelzang, A., Miyajima, M., Sugiura, Y., Wu, Y., Chamoto, K., Nakano, R., Hatae, R., Menzies, R.J., Sonomura, K., et al. (2021). B cell-derived GABA elicits IL-10(+) macrophages to limit anti-tumour immunity. Nature *599*, 471-476. 10.1038/s41586-021-04082-1.

Zhu, F., Feng, M., Sinha, R., Murphy, M.P., Luo, F., Kao, K.S., Szade, K., Seita, J., and Weissman, I.L. (2019). The GABA receptor GABRR1 is expressed on and functional in hematopoietic stem cells and megakaryocyte progenitors. Proc Natl Acad Sci U S A *116*, 18416-18422. 10.1073/pnas.1906251116.

457 **Figure legends**

458 **Figure 1. B cells are a source of GABA in the bone marrow.**

459 (A) Representative flow plots showing the emergence of B lineage cells in the OP9 co-culture.

460 (B) Schematic of HSPC OP9 B cell differentiation co-culture.

461 (C) Left: Quantification of the percentage of Cd19+ B cells at different timepoints; Right: mass

462 spectrometric quantification of GABA level in the media throughout B cell differentiation.

463 (D) Breeding scheme to generate *Cd19-Cre;Gad1/2*$^{fl/fl}$*;Rosa26*^{tdTomato} mice and control mice.

464 (E) Left: Quantification of B cells produced during differentiation of HSPCs; Right: GABA

465 level in the media from *Cd19-cre;Gad1/2*$^{fl/fl}$*;Rosa26*^{tdTomato} mice and WT mice at Day 12.

466 (F) Mass spectrometric quantification of GABA in *Cd19-cre;Gad1/2*$^{fl/fl}$*;Rosa26*^{tdTomato} and

467 control mouse femur (n = 5 mutants vs n = 5 control).

468 (G) Left: Representative flow plots showing the HSPC gates (Lin-/Sca-1+/c-Kit+); Right:

469 Quantification of LSK cell abundance in *Cd19-cre;Gad1/2*$^{fl/fl}$*;Rosa26*^{tdTomato} mice and

470 control mice (n = 9 mutants vs n = 9 control). Data is represented as mean ± SEM (*$p<0.05$,

471 **$p<0.01$, ***$p<0.001$, ****$p<0.0001$), Welch's test and one-way ANOVA with Tukey's

472 test were performed.

473 **Figure 2. Bone marrow endothelial cells are a source of GABA in bone marrow niche.**

474 (A) Breeding scheme to generate *Cdh5-CreERT2;Gad1/2*$^{fl/fl}$*;Rosa26*^{tdTomato} mice and control

475 mice.

476 (B) Mass spectrometric quantification of GABA in *Cdh5-CreERT2;Gad1/2*$^{fl/fl}$*;Rosa26*^{tdTomato}

477 and control mouse femur (n = 3 mutants vs n = 3 control).

478 (C) Left: Representative flow plots showing the HSPC gates (Lin-/Sca-1+/c-Kit+); Right:
479 Quantification of LSK cell abundance in *Cdh5-CreERT2;Gad1/2*$^{fl/fl}$*;Rosa26*^{tdTomato} mice
480 and control mice (n = 11 mutants vs n = 12 control). Data is represented as mean ± SEM
481 (*p<0.05, **p<0.01), Welch's test was performed.

482 **Figure 3. BMEC and hematopoietic cell-derived GABA coordinates to regulate HSPC**
483 **activity.**

484 (A) Breeding scheme to generate *Tie2-Cre;Gad1/2*$^{fl/fl}$*;Rosa26*^{tdTomato} mice and control mice.
485 (B) Mass spectrometric quantification of GABA in *Tie2-Cre;Gad1/2*$^{fl/fl}$*;Rosa26*^{tdTomato} and
486 control mouse femur (n = 3 mutants vs n = 3 control).
487 (C) Left: Representative flow plots showing the HSPC gates (Lin-/Sca-1+/c-Kit+); Right:
488 Quantification of LSK cell abundance in *Tie2-Cre;Gad1/2*$^{fl/fl}$*;Rosa26*^{tdTomato} mice and
489 control mice (n = 7 mutants vs n = 7 control).
490 (D) Percentage of B220+ cells in the peripheral blood in *Tie2-Cre;Gad1/2*$^{fl/fl}$*;Rosa26*^{tdTomato}
491 mice and control mice (n = 9 mutants vs n = 9 controls). Data is represented as mean ±
492 SEM (*p<0.05), Welch's test was performed.

493 **Figure 4. Reduction in GABA level induced transcriptional changes in HSPCs.**

494 (A) Heatmap of hierarchical clustering based on differentially expressed genes in *Gad1/2*$^{fl/fl}$
495 mutant models, (|logFC| >1, FDR < 0.1).
496 (B) Venn diagram of genes that were commonly or differentially expressed in *Gad1/2*$^{fl/fl}$ mutant
497 models.
498 (C) Heatmap of the expression level of 21 genes that were commonly upregulated in *Gad1/2*$^{fl/fl}$
499 mutant models.

500 (D) GSEA enrichment plots showing upregulated pathways in *Gad1/2*$^{fl/fl}$ mutant models.

501 (E) GSEA enrichment plots showing downregulated pathways in *Gad1/2*$^{fl/fl}$ mutant models.

502 (F) Schematic of HSPC OP9 B cell differentiation co-culture with 2-OH-Saclofen or vehicle

503 control added. Quantification of B cells produced in OP9 co-culture supplemented with

504 different concentrations of 2-OH-Saclofen. Data is represented as mean ± SEM (**p<0.01,

505 ***p<0.001), one-way ANOVA with Tukey's test were performed.

506 **Supplementary Figure 1. Genetic knockout efficiency in Gad1/2$^{fl/fl}$ mutants.**

507 (A) Gad1 genetic knockout efficiency shown by the percentage of tdTomato+ CD19+ cells in

508 *Cd19-Cre;Gad1/2*$^{fl/fl}$*;Rosa26*^{tdTomato} mice.

509 (B) Gad1 genetic knockout efficiency shown by the presence of tdTomato+ cells in the whole

510 BM cells in *Cdh5-CreERT2;Gad1/2*$^{fl/fl}$*;Rosa26*^{tdTomato} mice.

511 (C) Gad1 genetic knockout efficiency shown by the percentage of tdTomato+ cells in the whole

512 BM cells in *Tie2-Cre;Gad1/2*$^{fl/fl}$*;Rosa26*^{tdTomato} mice.

513 **Supplementary Figure 2. Hematopoietic profiles of Gad1/2$^{fl/fl}$ mutants.**

514 (A) Total BM cells from 1 femur and 1 tibia in *Cd19-Cre;Gad1/2*$^{fl/fl}$*;Rosa26*^{tdTomato} and control

515 mice (n = 9 mutants vs n = 9 control).

516 (B) Quantification of B220+ cell percentage in the PB in *Cd19-Cre;Gad1/2*$^{fl/fl}$*;Rosa26*^{tdTomato}

517 mice and control mice (n = 3 mutants vs n = 3 control).

518 (C) Quantification of BM B220+ cells in *Cd19-Cre;Gad1/2*$^{fl/fl}$*;Rosa26*^{tdTomato} mice and control

519 mice (n = 9 mutants vs n = 9 control).

520 (D) Total BM cells from 1 femur and 1 tibia in *Cdh5-CreERT2;Gad1/2*$^{fl/fl}$*;Rosa26*^{tdTomato} mice

521 and control mice (n = 12 mutants vs n = 12 control).

522 (E) Quantification of common lymphoid progenitors (CLPs; Lin-/Sca-1-lo/c-Kit-
523 lo/CD127+/CD135+) in *Cdh5-CreERT2;Gad1/2*$^{fl/fl}$*;Rosa26*^{tdTomato} and control mice (n = 6
524 mutants vs n = 6 control).
525 (F) Percentage of B220+ cells in the PB in *Cdh5-CreERT2;Gad1/2*$^{fl/fl}$*;Rosa26*^{tdTomato} mice and
526 control mice (n = 9 mutants vs n = 7 controls).
527 (G) Quantification of BM B220+ cell in *Cdh5-CreERT2;Gad1/2*$^{fl/fl}$*;Rosa26*^{tdTomato} mice and
528 control mice (n = 12 mutants vs n = 12 control).
529 (H) Percentage of CD11b+ cells in the PB in *Cdh5-CreERT2;Gad1/2*$^{fl/fl}$*;Rosa26*^{tdTomato} and
530 control mice (n = 6 mutants vs n = 5 control).
531 (I) Total BM cells from 1 femur and 1 tibia in *Tie2-Cre;Gad1/2*$^{fl/fl}$*;Rosa26*^{tdTomato} mice and
532 control mice (n = 7 mutants vs n = 7 control).
533 (J) Quantification of CLPs (Lin-/Sca-1-lo/c-Kit-lo/CD127+/CD135+) in *Tie2-*
534 *Cre;Gad1/2*$^{fl/fl}$*;Rosa26*^{tdTomato} and control mice (n = 7 mutants vs n = 7 control).
535 (K) Quantification of BM B cell abundance in *Tie2-Cre;Gad1/2*$^{fl/fl}$*;Rosa26*^{tdTomato} mice and
536 control mice (n = 12 mutants vs n = 12 control).
537 (L) Percentage of CD11b+ cells in the PB in *Tie2-Cre;Gad1/2*$^{fl/fl}$*;Rosa26*^{tdTomato} and control
538 mice (n = 9 mutants vs n = 9 control). Data is represented as mean ± SEM (*p<0.05),
539 Welch's test was performed.

540 **Supplementary Figure 3. Gene expression profiles of Gad1/2$^{fl/fl}$ mutants.**

541 (A) Distinct gene expression profiles of WT and *Gad1/2*$^{fl/fl}$ mutant models shown by PCA plot.
542 (B) Heatmap of normalized expression levels of B cell blueprint genes in *Gad1/2*$^{fl/fl}$ mutant
543 models.

544 (C) GSEA result showing top enriched GO terms in *Cd19-Cre;Gad1/2*$^{fl/fl}$*;Rosa26*^{tdTomato}

545 mutants.

546 (D) GSEA result showing top enriched GO terms in *Cdh5-CreERT2;Gad1/2*$^{fl/fl}$*;Rosa26*^{tdTomato}

547 mutants.

548 (E) GSEA result showing top enriched GO terms from *Tie2-Cre;Gad1/2*$^{fl/fl}$*;Rosa26*^{tdTomato}

549 mutants.

Supplementary Methods

Mass spectrometric detection of GABA

All solvents for processing and mass spectometry analysis were Optima LCMS grade from Fischer Scientific (Waltham, MA), unless otherwise noted. Individual bones were weighed and placed in a 2-ml screwcap tube pre-loaded with 2.8mm ceramic beads (Fischer Scientific, Pittsburgh PA). Ice cold 150 mM ammonium bicarbonate (Sigma Aldrich, St. Louis MO) was added (5 mls/gram of tissue) and samples were placed on ice. Samples were then homogenized in an Omni 48-place bead mill homogenizer (Omni International, Kennesaw, GA) set to 6m/sec for 30 sec. Sample homogenization was repeated twice more to fully disrupt bone tissue placing samples on ice between replicates. Following processing 50 µl of bone homogenate was transferred to a 1.7 ml microcentrifuge tube and precipitated with 200 µl ACN/1% formic acid containing internal standard, d_6-g-aminobutyric acid, (CDN resource laboratories Langley, BC). To remove insoluble material the samples were spun in a refrigerated centrifuge at 20,000 xg for 15 mins. The supernatant was filtered in a prewashed 96-well format Sirocco plate (Waters Corp. Milford, MA) into a 1-ml receiver plate according to the manufacturer's protocol. The plate was then dried under nitrogen. Samples were resuspended in 150 ul 1% formic acid for LC/MS/MS analysis. Calibrators (0.75 ng/ml-500 ng/ml) and QC samples for g-aminobutyric acid (Sigma Aldrich, St. Louis MO) were prepared in water, as GABA free bone matrix is not available. The calibrators and QC samples were processed in tandem with unknown samples (addition of ISTD, precipitation and filtration).

For quantitative analysis samples, QCs and calibrators were injected in random order onto a 150 mM Intrada Amino Acid Column (Imtakt, Portland OR) using a Waters Acquity I-Class UPLC system (Waters, Milford MA). The column was held at 60 °C and the flow-rate was 0.500 ml/min.

Analytes were eluted from the column using a gradient. Solvent A was water/0.1% FA and solvent B was ACN/0.1% FA. Briefly, 7.5 µl of sample was injected at 30% B and the %B was ramped to 75% B in 5.5 minutes, then to 99% in 0.2 min. The %B was held at 99% for 1.3 minutes before returning to 30% in 0.2 min followed by a re-equilibration hold at 1.2 minutes before injection of the next samples. Eluate from the column was analyzed in positive ion mode using a QTrap 5500 hybrid triple quadrupole mass spectrometer (SCIEX, Framingham MA) operating in multiple-reaction-mode (MRM) under conditions optimized for detection of the analyte and internal standard. For g-aminobutyric acid the transitions were: parent ion 104.05/product ions 87, 86 and 69. The transitions for d_6-g-aminobutyric acid: parent 110.09/product ions 93, 92.5 and 73.10. All transitions had a 50 msec dwell time. Triplicate injections of samples, calibrators and QCs were used for quantitative analysis allowing calculation of mean and standard deviation, blanks were run between each injection. The mean area under the curve (AUC) of the analyte relative to ISTD was used to construct a quadratic fit for the calibration curve in the MultiQuant software (SCIEX, Framingham, MA). Calibrators were excluded from quantitation models if their calculated concentrations were >15% different from theoretical. For all calibrators, samples, or QCs if the calculated %RSD of the triplicate injections was >15% samples were not considered valid.

All calibration curves had r-values $\geq$ 0.995. For all assays QC samples at each concentration fell within 15% of theoretical concentrations. The lower limit of detection was based on a signal to noise value of three (determined in MultiQuant). The lower limit of quantitation for each assay was based on either a signal to noise value of ten, or set at a g-aminobutyric acid concentration equal to the lowest concentration calibrator, whichever was higher. The upper limit of quantitation for each assay was set at the highest calibrator meeting the $\pm$15% of theoretical metric.

Graphical Abstract

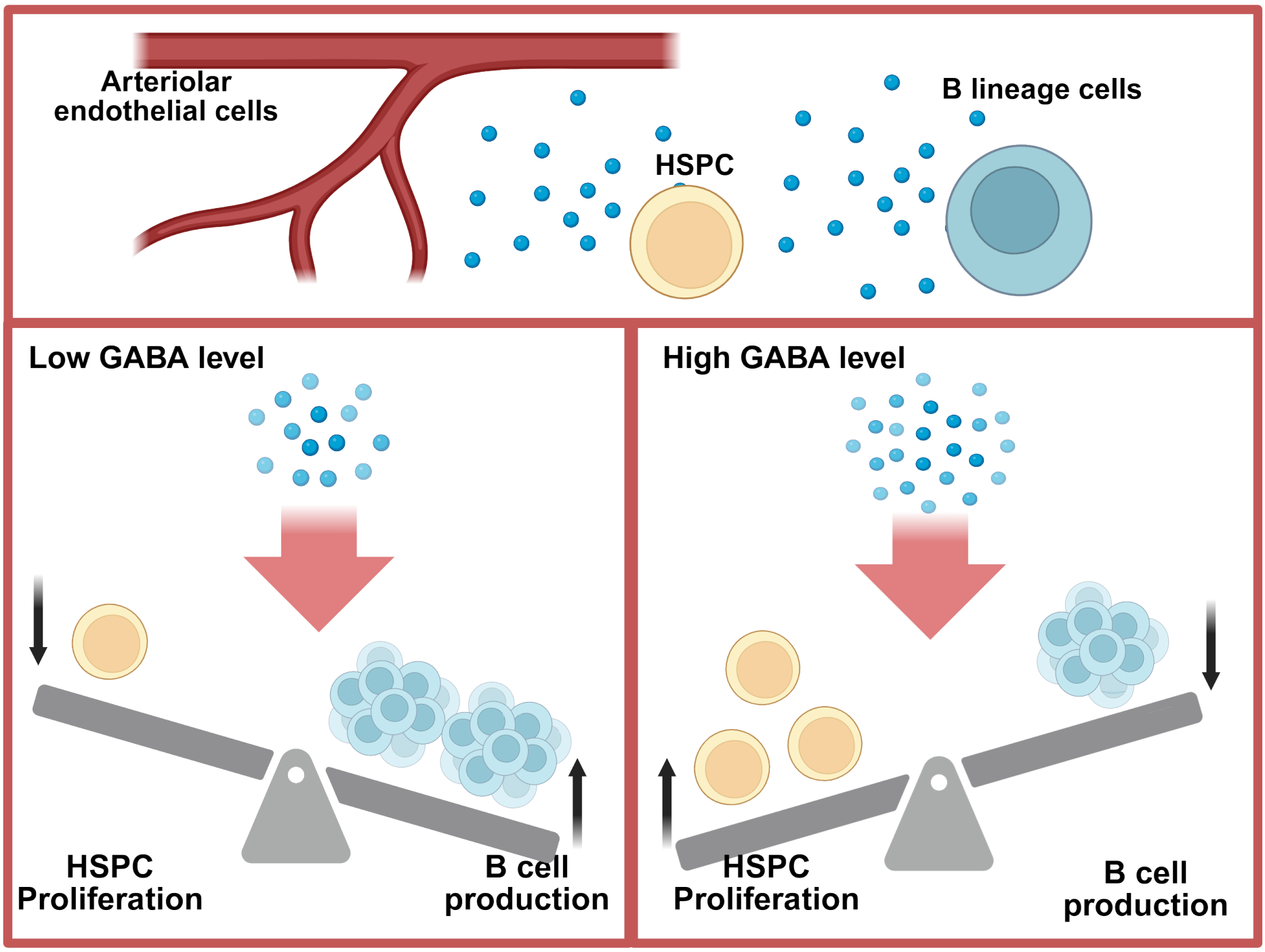

Figure 1

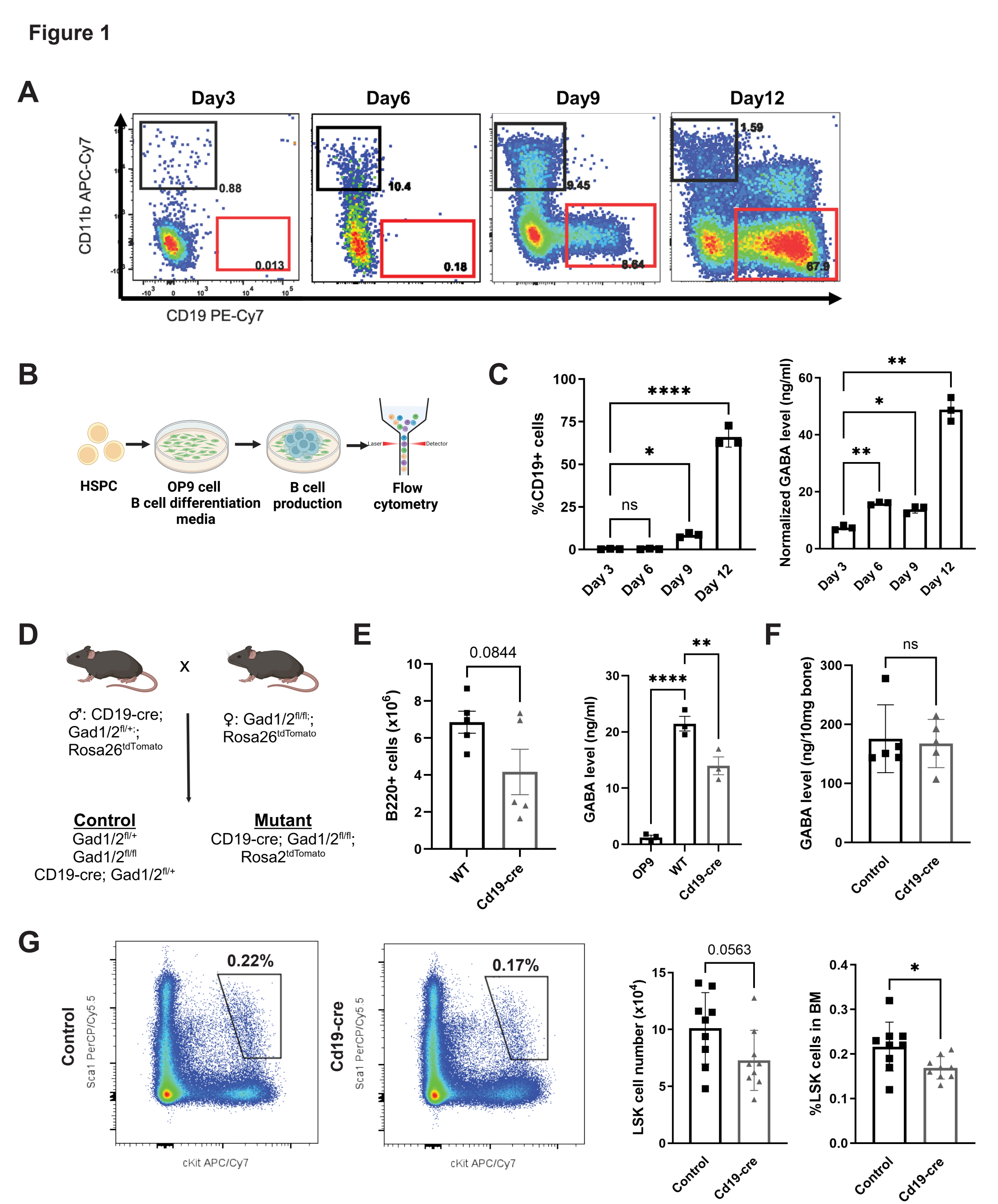
A
Day3
Day6
Day9
Day12
CD11b APC-Cy7
CD19 PE-Cy7
0.88
0.013
10.4
0.18
9.45
8.64
1.59
67.9
B
HSPC
OP9 cell
B cell differentiation media
B cell production
Flow cytometry
Laser
Detector
C
%CD19+ cells
Day 3
Day 6
Day 9
Day 12
ns
*
****
Normalized GABA level (ng/ml)
**
*
D
♂: CD19-cre; Gad1/2fl/+; Rosa26tdTomato
x
♀: Gad1/2fl/fl; Rosa26tdTomato
Control
Gad1/2fl/+
Gad1/2fl/fl
CD19-cre; Gad1/2fl/+
Mutant
CD19-cre; Gad1/2fl/fl; Rosa2tdTomato
E
B220+ cells (x10^6)
0.0844
WT
Cd19-cre
GABA level (ng/ml)
OP9
F
GABA level (ng/10mg bone)
ns
Control
G
Control
Cd19-cre
Sca1 PerCP/Cy5.5
cKit APC/Cy7
0.22%
0.17%
LSK cell number (x10^4)
0.0563
%LSK cells in BM

Figure 2

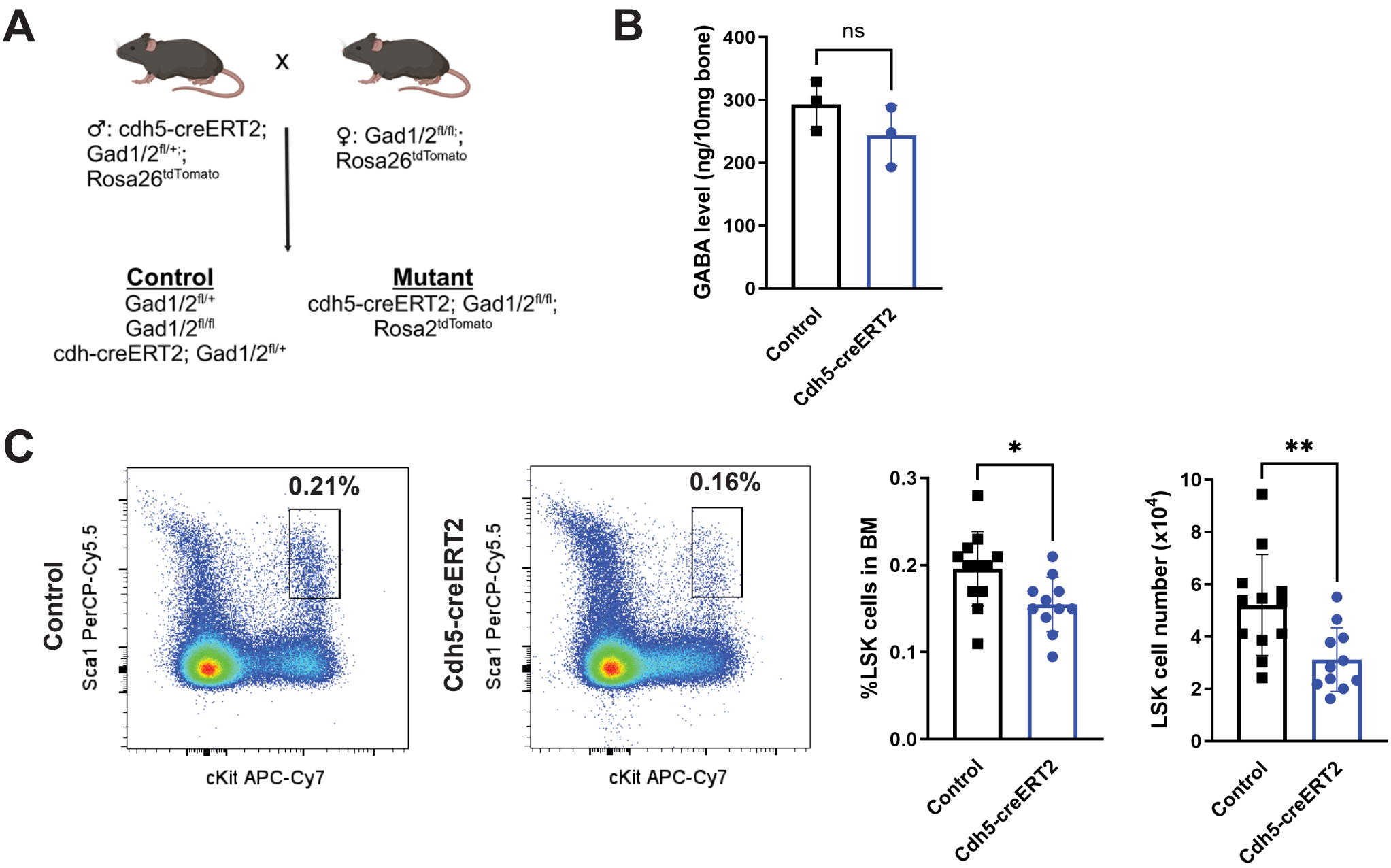
A
x
♂: cdh5-creERT2; Gad1/2fl/+; Rosa26tdTomato
♀: Gad1/2fl/fl; Rosa26tdTomato
Control
Gad1/2fl/+
Gad1/2fl/fl
cdh-creERT2; Gad1/2fl/+
Mutant
cdh5-creERT2; Gad1/2fl/fl; Rosa2tdTomato
B
ns
GABA level (ng/10mg bone)
400
300
200
100
0
Control
Cdh5-creERT2
C
Control
Cdh5-creERT2
Sca1 PerCP-Cy5.5
cKit APC-Cy7
0.21%
0.16%
%LSK cells in BM
0.3
0.2
0.1
0.0
*
LSK cell number (x10^4)
10
8
6
4
2
0
**
Control
Cdh5-creERT2

Figure 3

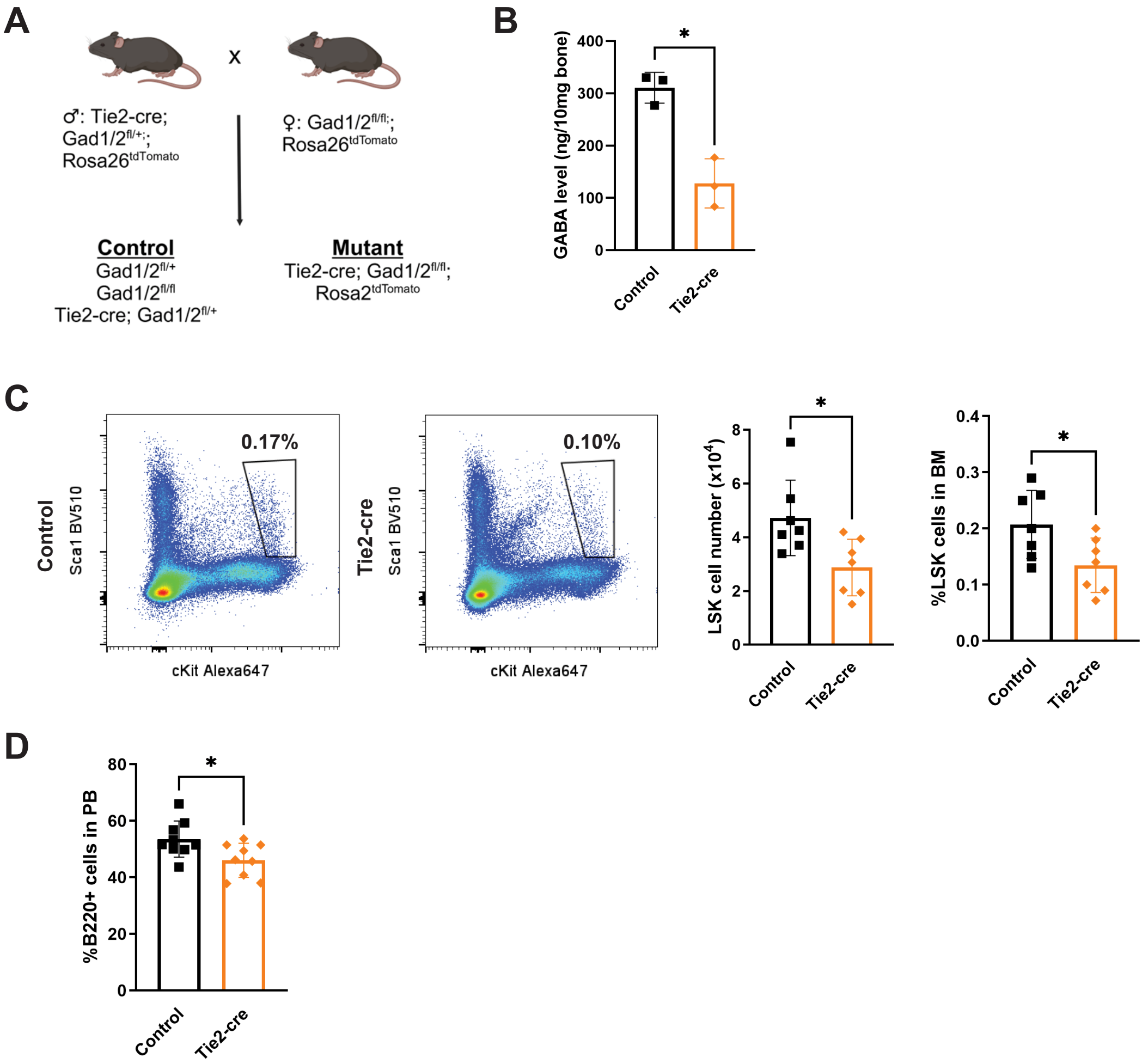
A
x
♂: Tie2-cre; Gad1/2fl/+; Rosa26tdTomato
♀: Gad1/2fl/fl; Rosa26tdTomato
Control
Gad1/2fl/+
Gad1/2fl/fl
Tie2-cre; Gad1/2fl/+
Mutant
Tie2-cre; Gad1/2fl/fl; Rosa2tdTomato
B
GABA level (ng/10mg bone)
400
300
200
100
0
*
Control
Tie2-cre
C
Control
Sca1 BV510
cKit Alexa647
0.17%
Tie2-cre
Sca1 BV510
cKit Alexa647
0.10%
LSK cell number (x10^4)
8
6
4
2
0
*
Control
Tie2-cre
%LSK cells in BM
0.4
0.3
0.2
0.1
0.0
*
Control
Tie2-cre
D
%B220+ cells in PB
80
60
40
20
0
*
Control
Tie2-cre

Figure 4

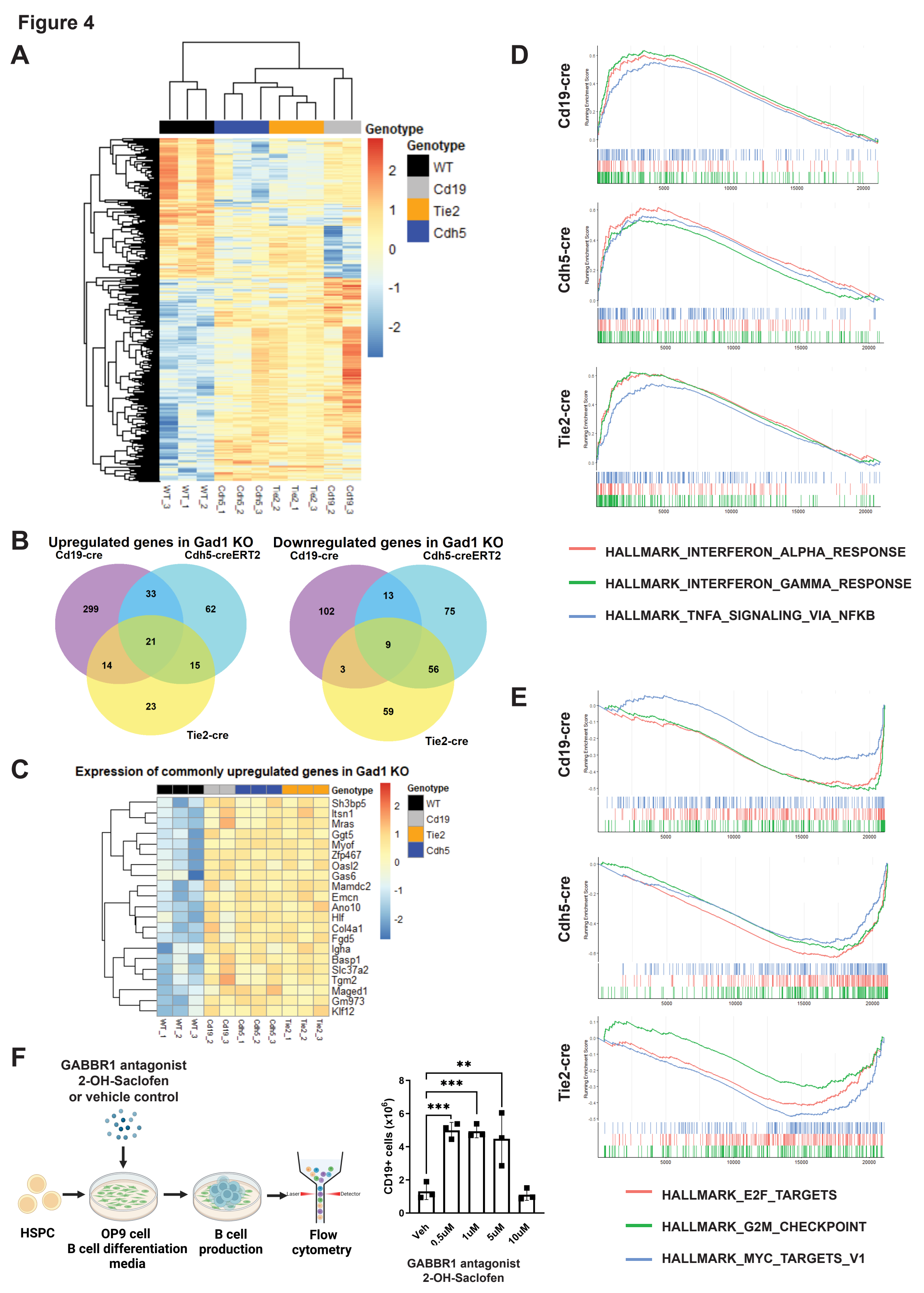
A
Genotype
WT
Cd19
Tie2
Cdh5
2
1
0
-1
-2
WT_3
WT_1
WT_2
Cdh5_1
Cdh5_2
Cdh5_3
Tie2_2
Tie2_1
Tie2_3
Cd19_2
Cd19_3
B
Upregulated genes in Gad1 KO
Cd19-cre
Cdh5-creERT2
Tie2-cre
299
33
62
21
14
15
23
Downregulated genes in Gad1 KO
Cd19-cre
Cdh5-creERT2
Tie2-cre
102
13
75
9
3
56
59
C
Expression of commonly upregulated genes in Gad1 KO
Sh3bp5
Itsn1
Mras
Ggt5
Myof
Zfp467
Oasl2
Gas6
Mamdc2
Emcn
Ano10
Hlf
Col4a1
Fgd5
Igha
Basp1
Slc37a2
Tgm2
Maged1
Gm973
Klf12
WT_1
WT_2
WT_3
Cd19_2
Cd19_3
Cdh5_1
Cdh5_2
Cdh5_3
Tie2_1
Tie2_2
Tie2_3
D
Cd19-cre
Cdh5-cre
Tie2-cre
Running Enrichment Score
5000
10000
15000
20000
HALLMARK_INTERFERON_ALPHA_RESPONSE
HALLMARK_INTERFERON_GAMMA_RESPONSE
HALLMARK_TNFA_SIGNALING_VIA_NFKB
E
Cd19-cre
Cdh5-cre
Tie2-cre
HALLMARK_E2F_TARGETS
HALLMARK_G2M_CHECKPOINT
HALLMARK_MYC_TARGETS_V1
F
GABBR1 antagonist
2-OH-Saclofen
or vehicle control
HSPC
OP9 cell
B cell differentiation
media
B cell
production
Laser
Detector
Flow
cytometry
CD19+ cells (x10^6)
**
***
***
Veh
0.5uM
1uM
5uM
10uM
GABBR1 antagonist
2-OH-Saclofen

Supplementary Figure 1

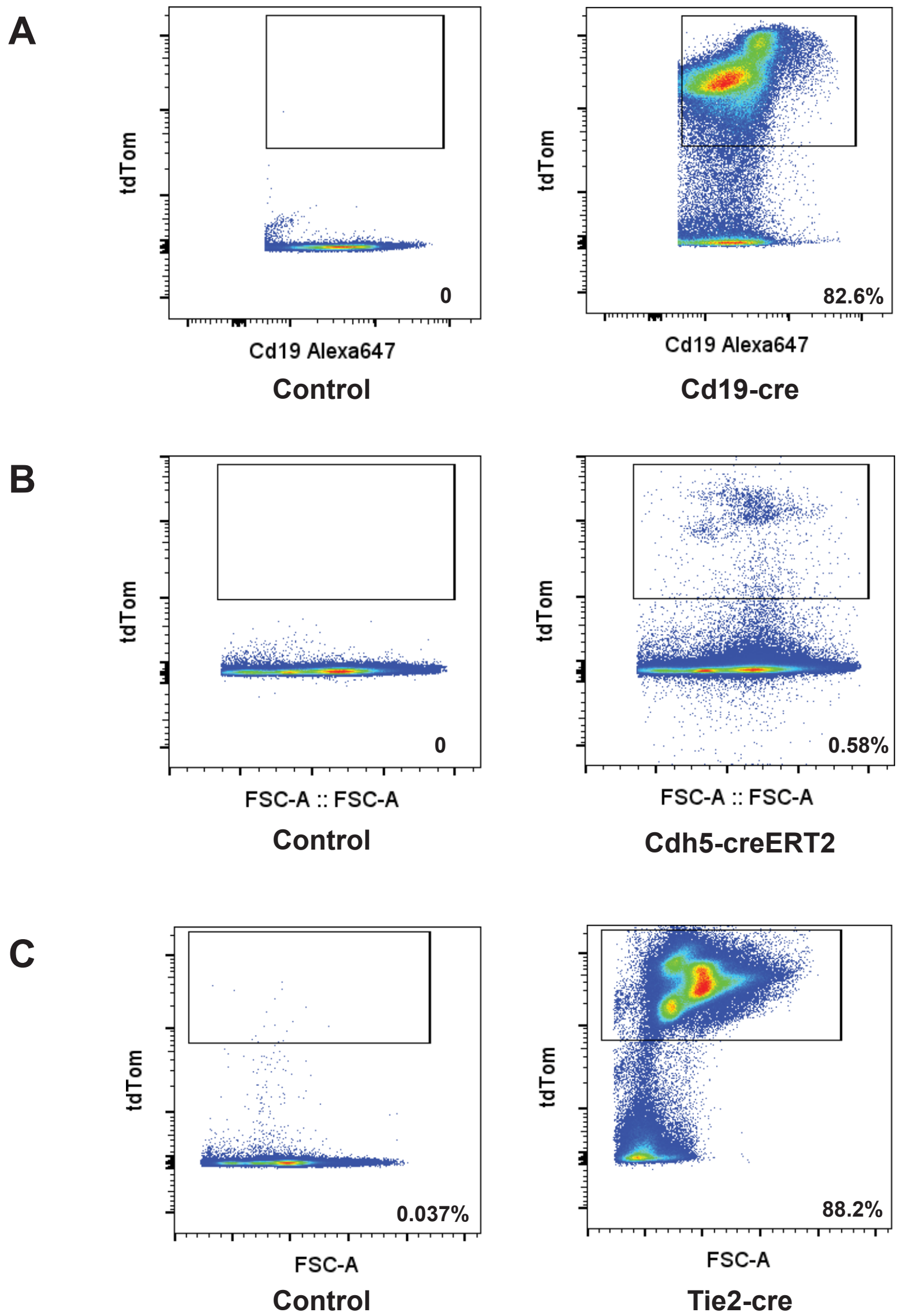

Supplementary Figure 2

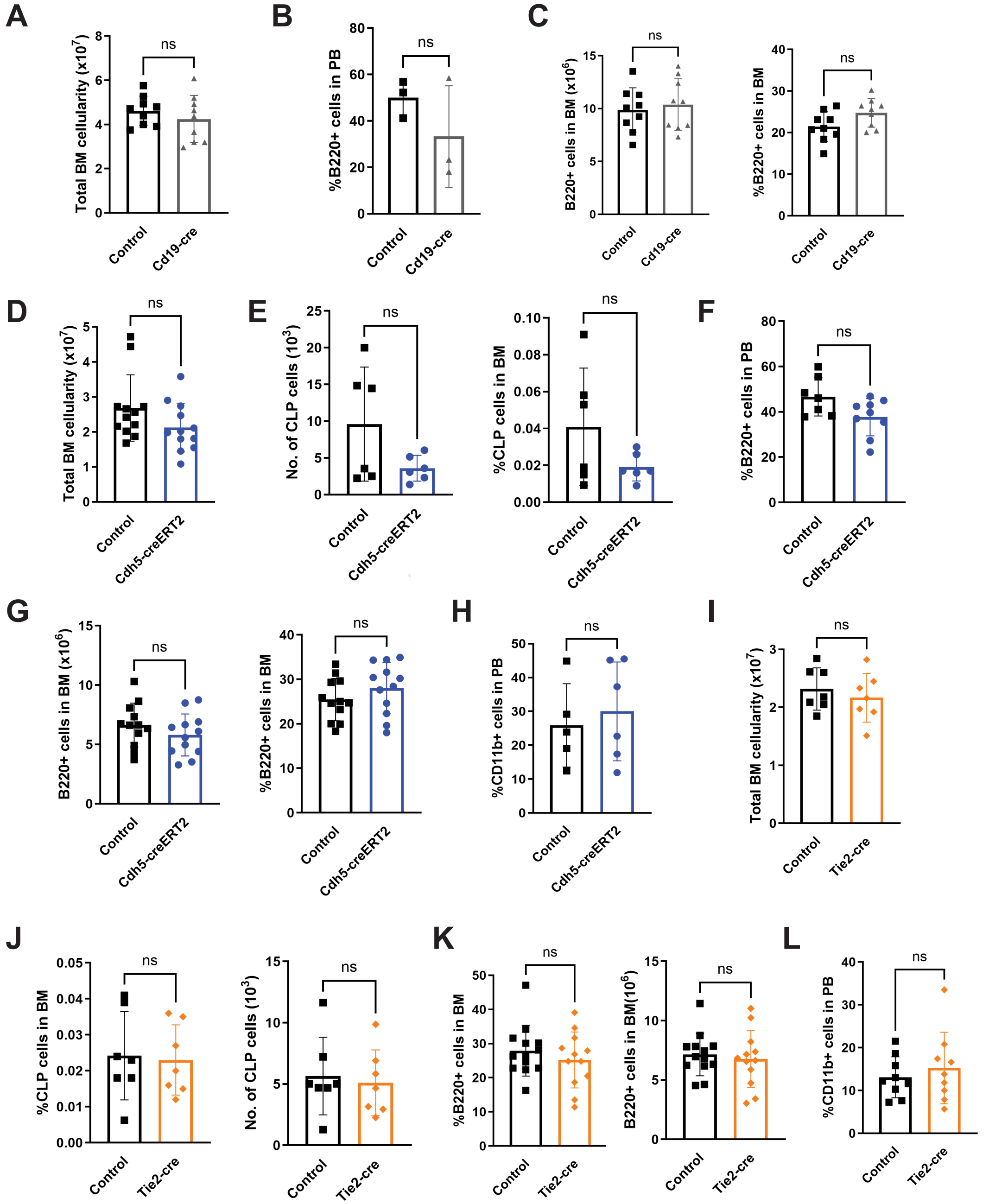

Supplementary Figure 3

A

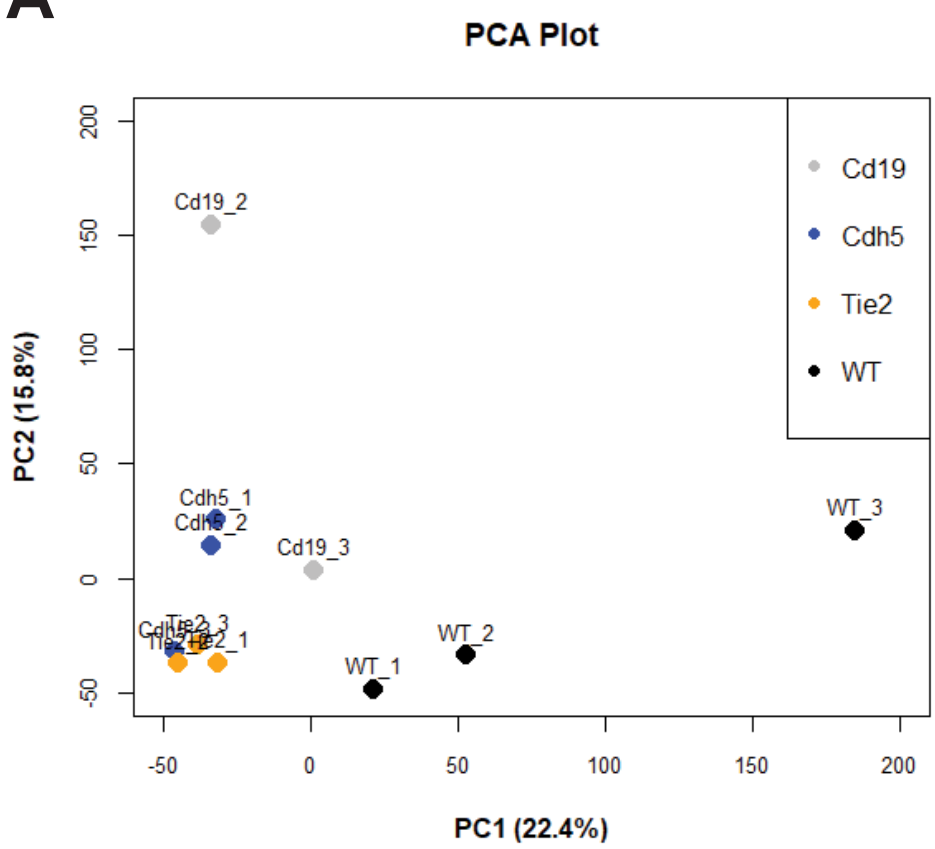

C

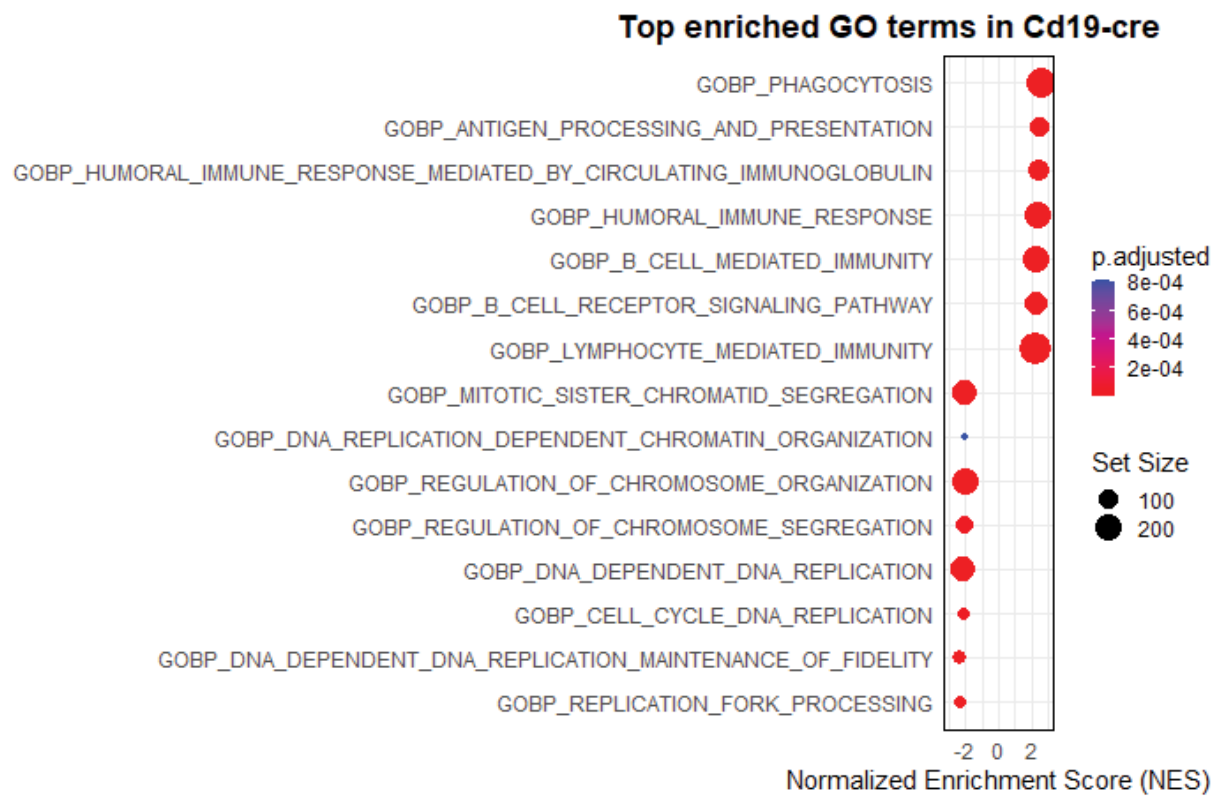

B

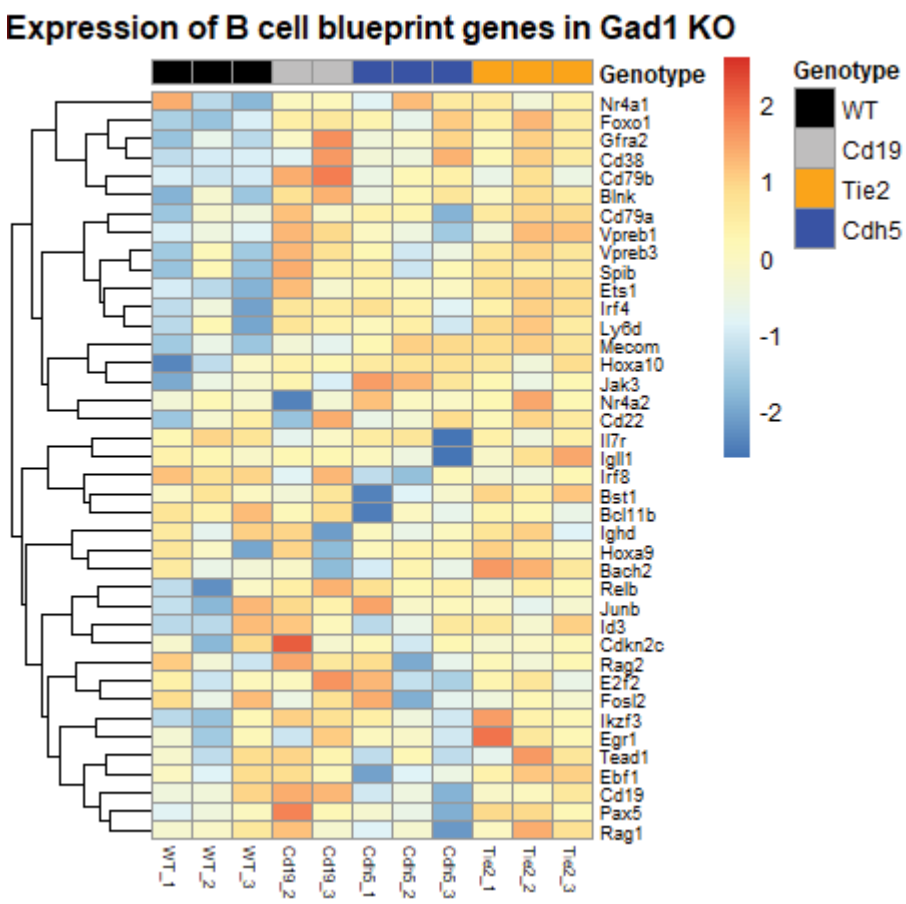

D

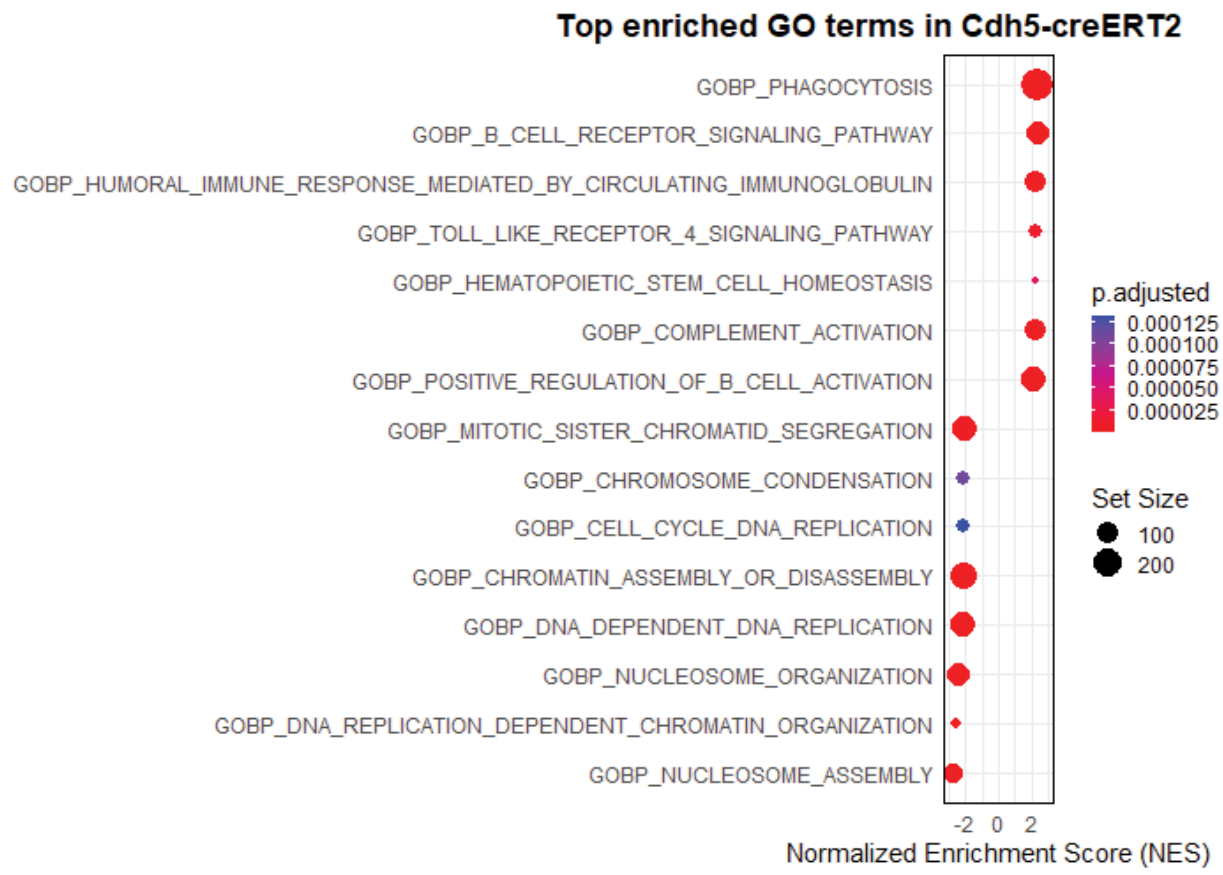
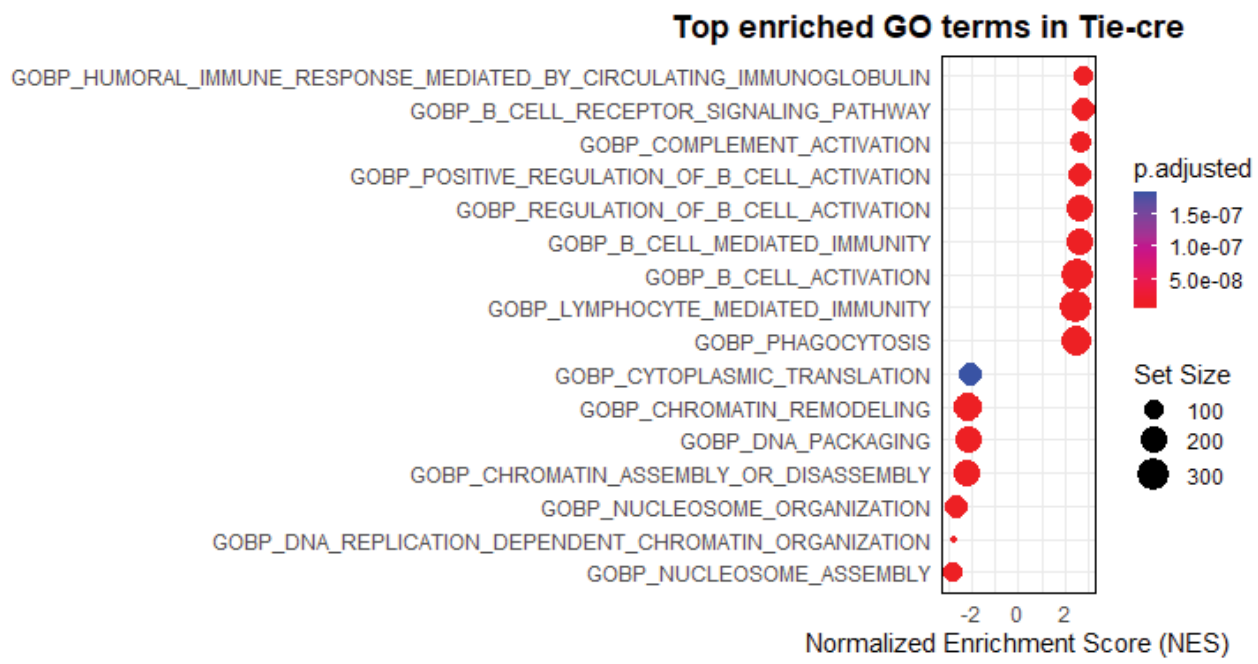
E